Atmos. Meas. Tech., 6, 2027–2041, 2013
www.atmos-meas-tech.net/6/2027/2013/
doi:10.5194/amt-6-2027-2013

Atmospheric Measurement Techniques
Open Access

An automated GC-C-GC-IRMS setup to measure palaeoatmospheric δ^{13}C-CH_4, δ^{15}N-N_2O and δ^{18}O-N_2O in one ice core sample

P. Sperlich[1,*], C. Buizert[1,], T. M. Jenk[1,***], C. J. Sapart[2], M. Prokopiou[2], T. Röckmann[2], and T. Blunier[1]**

[1]Centre for Ice and Climate (CIC), Niels Bohr Institute, University of Copenhagen, Copenhagen, Denmark
[2]Institute for Marine and Atmospheric Research in Utrecht (IMAU), University of Utrecht, Utrecht, The Netherlands
[*]now at: Max-Planck-Institute for Biogeochemistry (MPI-BGC), Jena, Germany
[**]now at: College of Earth, Ocean and Atmospheric Sciences, Oregon State University, Corvallis, USA
[***]now at: Paul Scherrer Institute, Villigen, Switzerland

Correspondence to: P. Sperlich (sperlich@nbi.ku.dk)

Received: 27 January 2013 – Published in Atmos. Meas. Tech. Discuss.: 28 February 2013
Revised: 26 June 2013 – Accepted: 6 July 2013 – Published: 13 August 2013

Abstract. Air bubbles in ice core samples represent the only opportunity to study the mixing ratio and isotopic variability of palaeoatmospheric CH_4 and N_2O. The highest possible precision in isotope measurements is required to maximize the resolving power for CH_4 and N_2O sink and source reconstructions. We present a new setup to measure δ^{13}C-CH_4, δ^{15}N-N_2O and δ^{18}O-N_2O isotope ratios in one ice core sample and with one single IRMS instrument, with a precision of 0.09, 0.6 and 0.7 ‰, respectively, as determined on 0.6–1.6 nmol CH_4 and 0.25–0.6 nmol N_2O. The isotope ratios are referenced to the VPDB scale (δ^{13}C-CH_4), the N_2-air scale (δ^{15}N-N_2O) and the VSMOW scale (δ^{18}O-N_2O). Ice core samples of 200–500 g are melted while the air is constantly extracted to minimize gas dissolution. A helium carrier gas flow transports the sample through the analytical system. We introduce a new gold catalyst to oxidize CO to CO_2 in the air sample. CH_4 and N_2O are then separated from N_2, O_2, Ar and CO_2 before they get pre-concentrated and separated by gas chromatography. A combustion unit is required for δ^{13}C-CH_4 analysis, which is equipped with a constant oxygen supply as well as a post-combustion trap and a post-combustion GC column (GC-C-GC-IRMS). The post-combustion trap and the second GC column in the GC-C-GC-IRMS combination prevent Kr and N_2O interferences during the isotopic analysis of CH_4-derived CO_2. These steps increase the time for δ^{13}C-CH_4 measurements, which is used to measure δ^{15}N-N_2O and δ^{18}O-N_2O first and then δ^{13}C-CH_4. The analytical time is adjusted to ensure stable conditions in the ion source before each sample gas enters the IRMS, thereby improving the precision achieved for measurements of CH_4 and N_2O on the same IRMS. The precision of our measurements is comparable to or better than that of recently published systems. Our setup is calibrated by analysing multiple reference gases that were injected over bubble-free ice samples. We show that our measurements of δ^{13}C-CH_4 in ice core samples are generally in good agreement with previously published data after the latter have been corrected for krypton interferences.

1 Introduction

Methane (CH_4) and nitrous oxide (N_2O) are important long-lived greenhouse gases that play a significant role in Earth's radiative budget (Solomon et al., 2007). The analysis of ancient air as archived in air bubbles within the polar ice sheets has significantly improved the understanding of Earth's atmospheric and biogeochemical variability. Especially CH_4 records have been used as proxy on the extension of wetlands on the stability of marine clathrates as CH_4 source. On glacial timescales, periods of warmer climate in the Northern Hemisphere correlated with increased concentrations of CH_4 and N_2O in the atmosphere (Flückiger et al., 2004; Loulergue et al., 2008; Schilt et al., 2010). Moreover, the mixing

ratios of both gases have significantly increased during industrialization, largely due to human activities (Solomon et al., 2007). Atmospheric mixing ratios of 1774 and 319 ppb have been published in the last IPCC report for CH_4 and N_2O, respectively (Solomon et al., 2007). With the prospect of even further increasing mixing ratios and their impact on future climate, it is important to thoroughly understand the biogeochemical processes related to both gases.

Brenninkmeijer et al. (2003) describe how the isotope fractionation of specific source and sink processes affect the integrated isotopic composition of the respective trace gases in the atmosphere. In an inverse approach, ice core isotope records of CH_4 and N_2O provide distinct constraints on biogeochemical processes that can be linked to the variability observed in the CH_4 and N_2O mixing ratios on decadal to millennial timescales (Sowers et al., 2003, 2005; Sowers, 2006, 2009; Ferretti et al., 2005; Schaefer et al., 2006; Fischer at al., 2008; Bock et al., 2010b; Melton et al., 2011a; Sapart et al., 2012). Because ice core records of CH_4 and N_2O isotopic composition indicate the natural response of specific greenhouse gas sinks and sources to palaeoclimate changes, this information is of great interest to global warming predictions.

Here, we present a method to simultaneously measure $\delta^{13}C$ isotope ratios of CH_4 as well as $\delta^{15}N$ and $\delta^{18}O$ isotope ratios of N_2O in a single ice core, firn gas or atmospheric sample. By melting ice core samples under vacuum, between 20 and 50 mL STP (standard temperature and pressure) of air can be extracted from 200–500 g of ice for isotopic analysis. Alternatively, atmospheric samples and reference gases can be injected into the system. The system is highly automated and comprises custom made units to separate CH_4 and N_2O from the main air components (N_2, O_2, Ar) and other trace gases (CO_2, CO) before using a modified gas-chromatography combustion unit coupled to a single isotope ratio mass spectrometer (GC-C-IRMS) in continuous-flow mode for isotope ratio determination. The combustion unit converts CH_4 to CO_2 so that the $\delta^{13}C$-CH_4 is measured as $\delta^{13}C$-CO_2 on the triple collector system of a mass spectrometer (Merritt et al., 1995). Our system includes permanent oxidation, a post-combustion cryo-trap and a second GC column, similar to Melton et al. (2011b). This GC-C-GC-IRMS method ensures a stable oxidation of the combustion reactor with minimized oxygen load into the IRMS, and it excludes interferences of the $\delta^{13}C$-CH_4 measurement with Kr inside the IRMS (Schmitt et al., 2013). The system is anchored to the international isotope scales using reference gases that were synthesized after Sperlich et al. (2012) for $\delta^{13}C$-CH_4 or calibrated by intercomparison measurements with two external laboratories for $\delta^{15}N$-N_2O and $\delta^{18}O$-N_2O. A novelty of this system is the isotope analysis of two isobaric gas species (CH_4-derived CO_2 and N_2O) from one ice core sample using one mass spectrometer in an online measurement mode. Furthermore, we introduce a gold catalyst for quantitative oxidation of CO which – to our knowledge – has hitherto not been used in setups for atmospheric measurements. We suggest the presented system as a powerful tool to provide high-precision isotopic analysis of palaeoatmospheric CH_4 and N_2O.

2 Methods

2.1 Extraction system

The extraction unit (Fig. 1) represents the interface for sample and reference gas introduction into the analytical setup and it includes the first step to separate the analytes from the main air components (N_2, O_2 and Ar). The sample lines of the extraction system are made of 1/4″ stainless steel (SST) tubes and Swagelok components (Swagelok, USA) except for the two six-port valves (V1 and V2) that are manufactured by VICI (VICI, USA) and connected to 1/16″ SST tubing. All connections are either welded or sealed with metal gaskets to exclude artefacts due to out-gassing of polymer gaskets (Sturm et al., 2004). All analytical lines are either continuously flushed by helium (He, 99.9995 %, Air Liquide, Denmark) or permanently evacuated by the turbo-pump (Pfeiffer, Germany).

The gas manifold enables the injection of gas from up to four different gas tanks or sample flasks into the extraction unit via a mass flow controller (referred to as MFC, manufactured by MKS, model 1179A, specified for N_2, 200 mL min^{-1}). A 100 mL sample volume parallel to the MFC enables aliquotation by expansion of gases from the gas manifold into the volume. The pressure reading of gauge "P1" (Keller, 21Y, max. 2 bar) is used to calculate the amount of air in the sample volume. We use two principle methods to introduce samples:

1. Ice core samples are placed in the 1.25 L melt vessel (SST glass adapter, DN 100, MDC vacuum, UK). Reference gases or air from flask samples can also be introduced into the melt vessel or into the water trap (T1) using manual valves and either the MFC or the sample volume. T1 comprises a 20 cm DN 50 SST tube that is welded to a quick flange connector and sealed with an aluminium gasket. Both 1/4″ tubes connecting the water trap are welded onto the opposing quick flange cap. The water trap is filled with glass beads of 3 mm diameter and cooled with a dry-ice/ethanol bath to −78 °C. The second pressure gauge "P2" (Edwards APG100-LC, minimum pressure 10^{-4} mbar) is mounted between T1 and the air-extraction trap (T2) to monitor vacuum and extraction efficiency. The gases can be extracted from the vacuum-extraction line by adsorbing the gases into T2 holding 1.5 g Hayesep D (60/80 mesh, Sigma-Aldrich) when submerged in liquid nitrogen (LN_2). Intensive extraction tests using several charcoal adsorbents (e.g. Norit RO and Fluka 05112, both from Sigma-Aldrich) in T2 showed additional CH_4

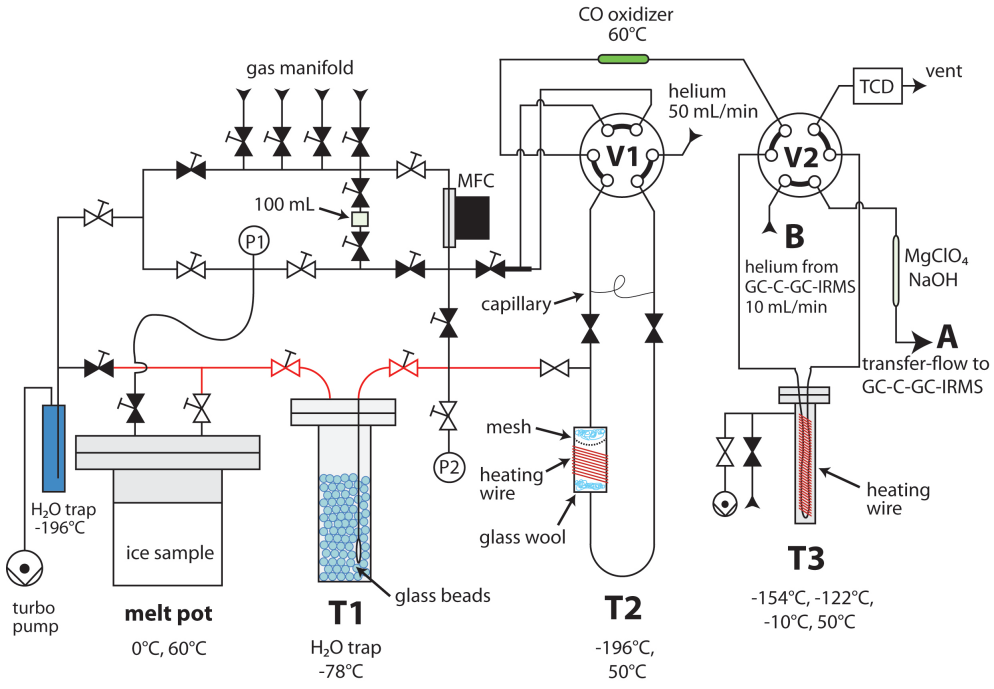

Fig. 1. Extraction unit design and flow scheme. Valve symbols with a handle symbolize manually operated valves, while symbols without a handle indicate automatically actuated valves. Filled valve symbols indicate closed valves; open symbols represent open valves. The figure shows the valve positioning of the extraction line during the melt extraction of an ice core sample. The red lines mark the section of the extraction unit which is thermally insulated and heated to 55 °C. The letters A and B identify the ports of V2 that are connected to the respective port A at V5 and port B at V4 of the GC-C-GC-IRMS setup (Fig. 2). Port A transfers the sample to the GC-C-GC-IRMS unit, while port B receives the carrier-gas flow for A.

contribution and high δ^{13}C-CH_4 variability. We also found that the speed of adsorption can be increased by a factor of 10 when the diameter of the adsorbing trap is increased from 6 to 15 mm. T2 is therefore built from a SST housing (ID $\sim$ 15 mm, F-type filter, Swagelok) welded to a U-shaped 1/4″ SST tube. A concave-shaped SST mesh doubles the area cross section of Hayesep D. Glass-wool plugs on top of the mesh and below the Hayesep D hold the adsorbent in place. T2 adsorbs about 200 mL air (STP) from the extraction line in less than 15 min, and has a maximum absorption capacity of $\sim$ 1.5 L (STP). The trap is equipped with a PID-controlled (proportional-integral-derivative) heating wire (4 m, 12.5 Ω m^{-1}, Type 1 NC 1, Thermocoax) that heats the trap to 50 °C when an automated lift removes the LN_2 Dewar from T2. The air sample is then transported by the extraction flow (50 mL min^{-1} He). A capillary above T2 maintains a He flush flow of 2 mL min^{-1} when the valves of T2 towards V1 are closed (Fig. 1). The SST line and the valves that connect the melt vessel with T1 and T2 are thermally insulated and constantly held at 55 °C with a PID-controlled heating wire.

2. Alternatively, the MFC can inject gas from pressurized tanks into the extraction flow directly when V1 and the manual valves are set accordingly (Fig. 1).

For both sample introduction methods, the sample gas is transported by the extraction flow through the CO oxidizer. Our CO oxidizer is comprised of a 10 cm 1/4″ SST tube holding a gold catalyst over a length of 5 cm (Aurolite™, Au/TiO_2, Strem Chemicals) between two glass-wool plugs that are kept in place by SST meshes at both ends. The CO-oxidizer column is held at 60 °C by a PID-controlled heating wire. The CO oxidizer is followed by the separation trap (T3), which is a modification of the principle described by DesMarais (1978). Thirty centimetres of a 1/8″ SST tube are filled with Hayesep D (80/100 mesh, Sigma-Aldrich, Switzerland) and temperature-controlled to −153, −122, −10 and 50 °C (all $\pm$ 0.4 °C) using a PID-controlled heating wire and a Pt-1000 temperature sensor. This 1/8″ tube is routed through an airtight DN 40 SST-cylinder, which can be evacuated or filled with helium. The lower part of the DN 40 tube is submerged in LN_2. To cool T3, the heat conductivity between the Hayesep D-filled 1/8″ tube and the LN_2-cooled DN 40 tube is increased by pressurizing the latter with helium to 2.5 bar. When the trap is heated to −10 or 50 °C, the space between 1/8″ and DN 40 tube is evacuated. T3 retains CH_4, N_2O, CO_2 and Kr at temperatures

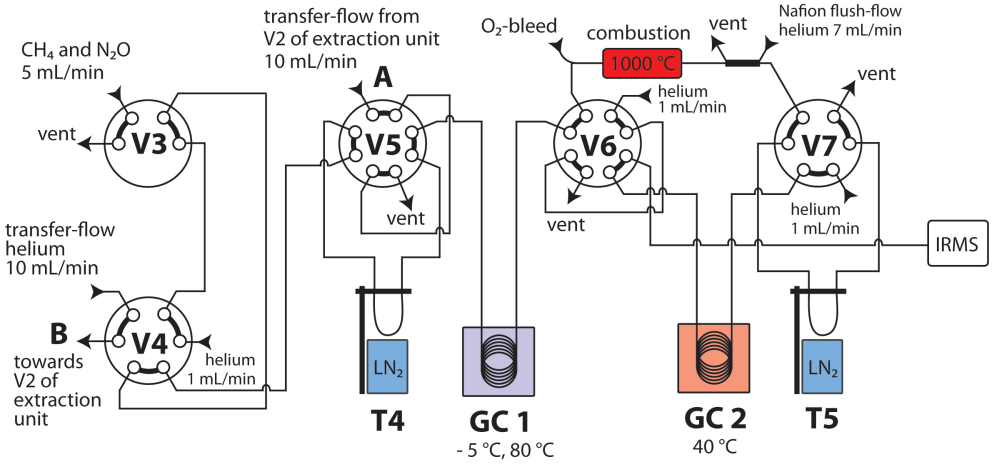

Fig. 2. Flow scheme of the GC-C-GC-IRMS unit. The letters A and B show the valve ports that connect to the ports A and B of the ice extraction unit, respectively. The CH_4 and N_2O sample is delivered to port A of the GC-C-GC-IRMS unit by the helium stream that flows out of the GC-C-GC-IRMS unit at port B.

$\leq -122\,°C$, while most N_2, O_2 and Ar pass through. The effluent of T3 is monitored with a thermal conductivity detector (micro-TCD, VICI) to enable CH_4 and N_2O mixing ratio analysis from TCD and IRMS peak areas. From T3, the sample is transported through a glass tube of 6 mm outer diameter (OD) and 600 mm length that holds Ascarite™ (NaOH, Sigma-Aldrich) to remove CO_2 and $Mg(ClO_4)_2$ (Merck) to remove H_2O.

2.2 GC-C-GC-IRMS system

The final purification and analysis of the air samples occurs via a combined GC-C-GC-IRMS setup (Fig. 2) after the ice core and air extraction unit. All valves are two-position VICI valves, and all tubing either 1/16″ SST tubes or fused silica capillaries. Valve V4 provides the transfer flow (10 mL min^{-1} He) and the analytical flow (1 mL min^{-1} He). Coming from T3, the sample is cryo-focussed on T4, a 55 cm section of GC-column (PoraBOND Q, 0.25 mm ID, Agilent) that can be submerged in LN_2. V4 allows for routing of either the transfer or the analytical flow through the injector valve V3 (2 µL, VICI, USA) for ∼ 1 nmol sized injections of pure CH_4 and N_2O into T3 or T4. These injections were used to tune the timing of the sequences and to monitor the reproducibility and drift during the test phase of the setup. The transfer flow from V4 to the ice extraction unit returns to valve V5 of the GC-C-GC-IRMS section (Fig. 2). This helium flow cryo-focuses the purified CH_4 and N_2O samples in T4. V5 then routes the analytical flow through T4 to introduce the sample gases into GC 1 (PoraBOND Q, 0.25 mm ID, 25 m length, Agilent). GC 1 is submerged in an ethanol bath at −5 °C to increase the chromatographic separation between CH_4 and N_2O to ∼ 160 s. GC 1 can be heated to 80 °C for desorption of H_2O. While it is possible to measure $\delta^{15}N$ and $\delta^{18}O$ in N_2O directly using GC-IRMS, CH_4 samples need to be combusted to CO_2 for $\delta^{13}C$ analysis (Merritt et al., 1995). The CH_4 elutes from GC 1 before N_2O and is routed to the combustion unit via V6. The combustion reactor contains three Ni wires (99.994 %), three Cu wires (99.9999 %) to store and provide oxygen during combustion and two Pt wires (99.997 %) to catalyse the combustion, (all wires are 0.1 mm OD, Alfa Aesar, UK). A small flow of oxygen is constantly added to guarantee maximum oxidation of the combustion reactor at all times in order to ensure a high CH_4 combustion rate (Cullis and Willatt, 1983). Water originating from the combustion process is removed by a Nafion membrane (60 cm length, TT-020, Perma Pure, USA) and a helium counter-flow of 7 mL min^{-1} at −5 °C. The eluting CH_4-derived CO_2 is trapped on T5 comprising of a fused silica capillary (350 µm ID, 55 cm length) submerged in LN_2. To increase the trapping efficiency and to prevent CO_2 loss, the capillary trap T5 contains a Ni wire (99.994 % Ni, 100 µm OD, Alfa Aesar), (e.g. Brand, 1995; Behrens et al., 2008). When the CH_4-derived CO_2 is trapped in T5, V6 redirects the GC flow to analyse the N_2O first. V6 and V7 are then switched, and T5 is removed from the LN_2 bath to pass the CH_4-derived CO_2 through GC 2, which is held at 40 °C (PoraBOND Q, 0.25 mm ID, 25 m length, Agilent) prior to measuring the CH_4-derived CO_2. Helium-flushed purge housings are used on valves V3–V6. The sample gases enter the IRMS (Delta V Plus, Thermo Fisher, Germany) through the open-split interface (ConFlo IV, Thermo Fisher, Germany). Before the N_2O- and CH_4-derived CO_2 samples are introduced into the IRMS, multiple "on/off" peaks of pure N_2O and CO_2 reference gases are applied to stabilize the IRMS (Sect. 3.2).

Table 1. Applied gases. Reference gas names are listed in column 1. Column 2, 3 and 4 show the calibration path for δ^{13}C-CH_4, the determined δ^{13}C and the mixing ratio of CH_4, respectively. The referencing path for N_2O is mentioned in column 5, while column 6, 7, and 8 indicate the δ^{15}N, the δ^{18}O and the mixing ratio of N_2O, respectively. The standard deviation for the isotopic composition of N_2O in GIS is larger compared to the other gases due to the calibration with two gases during measurements that were optimized to measure δ^{13}C-CH_4. The larger scatter results from the measurement of small N_2O amounts. Note that the mean value of the QCS measurements for the isotopic composition of N_2O proves very good accuracy for the calibration of GIS (Fig. 7).

Gas	referencing [CH_4]	δ^{13}C-CH_4 [‰]	[CH_4] [ppb]	referencing [N_2O]	δ^{15}N-N_2O [‰]	δ^{18}O-N_2O [‰]	[N_2O] [ppb]
GIS	RM-8563	-42.21 ± 0.04[a]	429	NEEM/AL	-1.05 ± 0.6	40.09 ± 0.5	345
NEEM	IMAU/Bern	-47.30 ± 0.01	1839	IMAU/[b]	6.49 ± 0.04	44.58 ± 0.06	322
AL	NEEM/GIS	-49.55 ± 0.16	716	IMAU/NEEM	1.01 ± 0.15	38.8 ± 0.4	272
NOAA	NEEM	-38.57 ± 0.05	1642	IMAU/NEEM	-0.46 ± 0.15	41.06 ± 0.4	332

The uncertainty estimates are based on the standard deviation (1σ) apart from [a], which is described by Sperlich et al. (2012). The [b] indicates when the referencing method of NEEM for the isotopic composition of N_2O is explained by Sapart et al. (2011).

2.3 Referencing to the isotope scales

We used four different reference gases in the described setup (Table 1). GIS (glacial isotope standard) refers to a synthetic air mixture that was prepared after Sperlich et al. (2012) with additional N_2O. An atmospheric air tank was sampled in the year 2008 at a clean-air site of the NEEM camp in northwest Greenland and is hereafter referred to as NEEM. Furthermore, we use two synthetic air mixtures called AL and NOAA that were provided by Air Liquide (Teknisk Luft, Air Liquide, Denmark) and the National Oceanic and Atmospheric Administration (NOAA, Boulder, USA), respectively.

The isotope ratios of all gas standards are referenced to the VPDB isotope scale for δ^{13}C-CH_4 and to the δ^{15}N scale of N_2 air and the δ^{18}O VSMOW scale for N_2O, respectively. The isotopic composition of N_2O in NEEM is prescribed by extrapolating the atmospheric trend between 1990 and 2002 (Röckmann and Levin, 2005) to July 2008, which is the sampling time of the NEEM cylinder. The integrity of our calibration scale for N_2O isotopic composition was tested by inter-calibration measurements of NEEM, AL and NOAA by the Institute for Marine and Atmospheric Research in Utrecht (IMAU), the Netherlands (published in Sapart et al., 2011). The isotopic composition of N_2O in GIS was referenced on the setup described in this paper by calibrating against NEEM and AL. The δ^{13}C-CH_4 in NEEM was calibrated by IMAU and the Institute for Climate and Environmental Physics at the University of Bern, Switzerland (Bern), (Jochen Schmitt, personal communication, 2011). GIS was independently referenced for δ^{13}C-CH_4 against RM 8563 (Verkouteren, 1999) with the δ^{13}C-CO_2 of RM 8563 assigned by Coplen et al. (2006). GIS was previously shown to be in excellent agreement with the externally calibrated NEEM air (Sperlich et al., 2012). AL was referenced for δ^{13}C-CH_4 on the described setup based on NEEM and GIS, while NOAA was calibrated for δ^{13}C-CH_4 by NEEM only. The mixing ratios of CH_4 and N_2O in GIS, NEEM and AL were measured at the Max-Planck-Institute for Biogeochemistry (Armin Jordan and Bert Steinberg, personal communication, 2012), while NOAA was provided with certificates. GIS was chosen as working standard for ice core measurements due to the similar mixing ratio of CH_4. Air samples with higher CH_4 mixing ratios, atmospheric samples such as NOAA, firn air or atmospheric samples, were referenced against NEEM.

2.4 Measurement correction and referencing protocol

The ice core measurement routine is shown in Table 2 and the routine for atmospheric gases from air tanks is shown in Table 3. Blocks of three GIS measurements are bracketing the ice core sample and the quality control standard (QCS) measurements. For each reference gas measurement, 40 mL (STP) of GIS were extracted from T1. The offset between the average isotope ratio determined for each block, and the target isotope ratio assigned to GIS is considered to indicate the daily offset of the system to the international isotope scales, including the system drift between the beginning and the end of the measurement day. The isotope ratio measurements of the ice core samples and the quality control standards are corrected for the sample size offset (Sect. 3.7) first, and then for the system offset as determined by GIS according to Werner and Brand (2001).

2.5 Ice core sample and system preparation

Measurements of ice samples begin with cooling of the H_2O trap T1 in a dry-ice/ethanol bath. To increase the heat conduction within the glass bead bed, T1 is pressurized with helium to ~ 1500 mbar for ~ 2 h. GC 1 is placed in the ethanol bath at $-5\,^{\circ}$C if it has previously been heated to 80 °C. Meanwhile, ice core samples which are stored at $-25\,^{\circ}$C are prepared in the cold room at $-15\,^{\circ}$C. All surfaces of ice core samples are cleaned by removing the top 3–5 mm with a bandsaw. Attached saw dust is then removed with a scalpel

Table 2. Measurement sequence for ice core samples. A sequence for two ice core sample measurements comprises 11 extraction measurements. Column 2 describes the function of each extraction. Column 3 and 4 show the name and amount of the extracted sample, while column 5 specifies the way the samples are introduced and column 6 shows from which analytical component the respective sample is extracted, where MV stands for melt vessel.

extraction	function	name	amount	introduction	extracted from
1	reference gas	GIS	40 mL	MFC	T1
2	reference gas	GIS	40 mL	MFC	T1
3	reference gas	GIS	40 mL	MFC	T1
4	ice core sample	[...]	200–500 g	manual	MV
5	blank test	blank	–	–	MV
6	QCS	AL	30–50 mL	MFC	T1
7	ice core sample	[...]	200–500 g	manual	MV
8	blank test	blank	–	–	MV
9	reference gas	GIS	40 mL	MFC	T1
10	reference gas	GIS	40 mL	MFC	T1
11	reference gas	GIS	40 mL	MFC	T1

or brushed off while the ice sample is carefully checked for anomalous features. To prevent contamination by laboratory air and/or drill-fluid intrusion, cracked parts are removed from each sample. Also, layers with exceptionally high content of dust or soot particles were cut out to prevent artefacts (Rhodes et al., 2013). On average, 30 % is removed from each sample. The decontaminated ice sample and a glass-coated magnet stir bar are then placed inside the melt vessel, which is sealed with a copper gasket and fastened with 16 bolts to 25 Nm torque. Two samples are prepared and stored in a −20 °C chest freezer to be analysed the same day. The analytical system is finally prepared by evacuating T1 as well as all lines and pressure regulators of the atmospheric reference gases connected to the gas manifold (Fig. 1). The measurement routine is started when the pressure inside the extraction system reaches 10^{-3} mbar, indicating the system is sufficiently leak-tight and dried after previous analysis.

After every day of ice core measurements, the melt vessel is cleaned with ultra-pure water and detergent soap for laboratory glassware (Alconox™, USA), as suggested by Mitchell et al. (2011), before it is dried at 80 °C overnight. To remove trapped water from T1, it is heated to 150 °C with a PID-controlled heating sleeve. The elevated temperature of the extraction line (55 °C, Fig. 1) promotes the drying efficiency of the whole extraction line. Under vacuum, any water is rapidly transferred from the heated parts into the water trap (LN_2 cooled) close to the turbo-pump. This water trap can easily be opened to remove the water. With this method, we avoid opening the connectors in the extraction line.

Table 3. Measurement sequence for air samples from flasks or tanks. The presented sequence is used for triplet measurements of two samples, bracketed by reference gas triplets. Column 2 describes the function of the measured gas, which is described and quantified in column 3 and 4, respectively. Column 5 indicates that all samples are injected through the mass flow controller (MFC) directly into T3 or to be extracted from T1, as indicated in column 6.

extraction	function	name	amount	introduction	extracted from
1	reference gas	NEEM	40 mL	MFC	T1/T3
2	reference gas	NEEM	40 mL	MFC	T1/T3
3	reference gas	NEEM	40 mL	MFC	T1/T3
4	air sample 1	[...]	40 mL	MFC	T1/T3
5	air sample 1	[...]	40 mL	MFC	T1/T3
6	air sample 1	[...]	40 mL	MFC	T1/T3
7	reference gas	NEEM	40 mL	MFC	T1/T3
8	reference gas	NEEM	40 mL	MFC	T1/T3
9	reference gas	NEEM	40 mL	MFC	T1/T3
10	air sample 2	[...]	40 mL	MFC	T1/T3
11	air sample 2	[...]	40 mL	MFC	T1/T3
12	air sample 2	[...]	40 mL	MFC	T1/T3
13	reference gas	NEEM	40 mL	MFC	T1/T3
14	reference gas	NEEM	40 mL	MFC	T1/T3
15	reference gas	NEEM	40 mL	MFC	T1/T3

2.6 Measurement procedure

2.6.1 Ice core samples

In order to minimize the time between the measurements, samples are introduced into the extraction unit while the previous sample is analysed in the GC-C-GC-IRMS section of the setup. This results in a sample interval of only 42 min. Ice core samples and reference gases are treated as similar as possible in order to balance analytical effects during analysis, following the principle of identical treatment (Werner and Brand, 2001). However, one difference exists in the application and extraction of ice core and reference gas sample: the MFC is used to inject reference gas into T1, from where it is extracted into T2. In contrast, ice core samples release the air during melting inside the melt vessel from where the gas is continuously cryo-pumped through T1 into T2. This is the only gas-handling difference between ice core sample and reference gas. We tested for isotope fractionation effects based on the different gas handling but found no significant isotope fractionation in our setup (see Sect. 3.7). The continuous extraction technique minimizes the pressure and the time the gas is in contact with the melt water as to reduce gas dissolution.

Every analysis begins with the evacuation of the extracting unit. The thoroughly cooled T1 represents the cavity for reference gas extractions, and is evacuated for 6 min prior to reference gas introduction. To measure an ice core sample, the melt vessel is attached during the previous reference gas measurement so it can be evacuated for 20–30 min without

delaying the measurement routine. During this time, the melt vessel is cooled in an ice water bath to prevent the sample from melting ahead of schedule. The measurement routine then continues with cooling T2 in LN_2 for 8 min in preparation for the extraction of ice core air or reference gases. Towards the end of cooling T2, reference gases are injected into T1, or the ice bath under the melt vessel is replaced by a hot water bath (60 °C) to start melting the ice. When T2 has cooled for 8 min, the air extraction is started by opening the valve between T1 and T2 and the melt vessel for ice extractions. After 40 mL (STP) of reference gas have been extracted for 13 min, the pressure within the extraction unit (P2) decreased from 14 mbar to 0.07 mbar, indicating 99.5 % extraction efficiency. The pressure decrease during extractions is very reproducible, and only varies with the amount of air and the variable melting time of ice core samples. By ensuring that reference gas and ice core samples are extracted to similar pressures, isotope fractionation effects based on variable completeness of extraction cancel out. The IRMS operating software (ISODAT) is started as soon as the pressure in the extraction system is lower than 0.11 mbar (P2), thereby ensuring identical extraction efficiency for all samples.

When the extraction has ended, reference gases and samples are subject to identical analytical procedures, precisely timed by the ISODAT script. First, T3 is cooled to −154 °C within 1 min and is held constant by the PID controller. After T3 has cooled for 4 min, the extraction is stopped. T2 gets heated from −196 to 50 °C in less than 1 min, thereby desorbing the sample within the extraction flow and transferring the sample from T2 through the CO oxidizer to T3. T3 separates N_2, O_2 and Ar from the sample gas mixture and retains CH_4, N_2O, CO_2 and Kr on the Hayesep D. At the same time, the temperature of T3 is increased to −122 °C to improve the separation performance of T3 (Umezawa et al., 2009). Residual N_2, O_2 and Ar will be separated later in the GC-C-GC-IRMS section. The TCD signal to measure the amount of N_2, O_2 and Ar is recorded using a LabView script. The separation in T3 is completed after 400 s. V2 is then switched and T3 heated to −10 °C so the transfer flow can carry the desorbing trace gases through the chemical trap into the capillary trap T4, which was submerged in LN_2 10 s before. CH_4 and N_2O are focussed in T4 after 360 s, V2 is then switched and T3 heated to 50 °C to vent residual water. Next, V5 is switched and the analytical flow transports both sample gases from T4 through GC 1 as T4 gets lifted from the LN_2 bath. It takes about 220 s for the CH_4 to pass through GC 1 and to enter the combustion oven. After 200 s, the post-combustion trap T5 is lowered into a LN_2 bath to trap the CH_4-derived CO_2.

After 80 s of post-combustion trapping, all CH_4-derived CO_2 is trapped in T5, and V6 gets switched to route the analytical flow directly to the open split and the IRMS for the isotopic measurement of N_2O. Meanwhile, V7 gets switched to a pure helium flow of 1 mL min^{-1} to remove the oxygen from T5. When the N_2O measurement is completed, V6 gets switched to route the CH_4-derived CO_2 from T5 through GC 2 into the open split for isotopic analysis in the IRMS. In the mean time, T1 and T2 are evacuated in preparation for the following sample.

2.6.2 Air samples

The analysis of air samples is similar to the analysis of ice core samples, and differs only in the fully automated introduction of air samples if the samples are applied from pressurized vessels. Air tanks can be connected to the gas manifold where the MFC introduces the samples through V1 into the extraction flow (Fig. 1). A sample flow time of 90 s allows for the sample and helium flows to equilibrate before V2 is switched to direct the sample into the pre-cooled T3. After this point, the analysis is exactly the same as described in Sect. 2.6.1; however, only one sample is introduced and analysed at a time. If the air samples are at sub-ambient pressures, they are introduced to T2 through the sample volume to be extracted like the reference gases during ice core measurements.

2.6.3 Sampling for system blank

System blank tests are determined after every ice core sample extraction (Table 2). For this purpose, the valves of the extraction line get closed when the ice extraction is completed. The sample vessel with the extracted sample is thereby kept under vacuum, but it can collect air from potential leakage into the extraction unit. The extraction volume is then extracted for 5 min and processed as a regular sample.

3 Results and discussion

3.1 CO oxidizer

Using the post-combustion trap strictly requires the elimination of any potential interference of non-CH_4 gases (CO and CO_2) with the CH_4-derived CO_2 in the mass spectrometer. To exclude any spurious CO contribution, CO is quantitatively oxidized to CO_2 and then removed by the Ascarite trap (Fig. 1). Schütze reagent is often used in analytical setups to oxidize CO to CO_2 at room temperatures when the CO is to be analysed for its isotopic composition of $\delta^{13}C$ and $\delta^{18}O$ (e.g. Brenninkmeijer, 1993). Alternatively, Sofnocat or hopcalite can be applied as oxidation catalyst (e.g. Kato et al., 1999). However, the CO-oxidation efficiency of both catalysts decreases with increasing moisture content (McPherson et al., 2009). To our awareness, this is the first system described for atmospheric measurements using Aurolite as catalyst to oxidize CO to CO_2. The efficiency of Aurolite is reported to even improve with increasing moisture content in the sample gas stream (e.g. Date et al., 2002; McPherson et al., 2009), making it particular suitable for CO elimination in air extracted from melted ice core samples. Our CO oxidizer is heated to 60 °C to increase the CO oxidation

efficiency (Date et al., 2002), while the oxidation of CH_4 can be ruled out at temperatures below 130 °C (Walther et al., 2009). We chose Aurolite on TiO_2 support because of its superior conversion efficiency and gold particle stability compared to Al_2O_3 and ZnO (Walther et al., 2009).

To test the system, synthetic CH_4- and CO_2-free air with a CO mixing ratio of 350 ppb was mixed in the setup described by Sperlich et al. (2012). This air mixture was applied to the system with and without the CO oxidizer as well as with a trap holding Schütze reagent (iodine pentoxide, 99.99 %, Sigma-Aldrich) inside a 6 mm OD glass tube over a length of 150 mm. The timing of the GC-C-GC-IRMS system was adjusted to fully combust, trap and analyse the residual CO that eluted from GC 1. Note that the CO that was oxidized in the CO oxidizer or in the Schütze reagent was chemically trapped on the Ascarite trap (Fig. 1) and therefore not detected. A series of experiments with Aurolite showed no CO-derived CO_2 peak that exceeded the normal blank peak, while up to 90 % of the CO passed through the Schütze reagent unoxidized. Our tests suggest that Aurolite quantitatively oxidizes CO in atmospheric samples and is significantly more reliable to oxidize CO than commercial Schütze reagent, and it also has the benefit of being immune to moisture. Based on the gold nanoparticle size stability reported by Date et al. (2002) and Walther et al. (2009), and the fact that our CO oxidizer is in contact with far less than 1 L of air per measurement day, we expect the CO oxidizer to be stable for many years.

3.2 Preparing the IRMS for measurement of two different gases

While only a small fraction of the analyte molecules that enter the ion source of an IRMS get ionized and reach the detector, other sample molecules can be subject not only to unintended physical and chemical interactions with the analytical system itself but also with molecules of other gas species present in the analyser. Potential effects include system memory, adsorption and desorption of gases altering the background levels, ion reactions (Anicich, 1993), reactions enabled by the hot filament and a combination of all (Brand, 2004). Measuring two isobaric gases such as N_2O and CO_2 in the same sample on the same IRMS can reduce the precision significantly if the conditions inside the IRMS vary throughout the measurements (Carter and Barwick, 2011). To increase the stability of our analyser, we inject a large pulse of pure reference gas into the ion source for 1 min before the start of each measurement sequence. The following measurement sequences are comprised of 10 or 12 flat-topped peaks of pure CO_2 or N_2O reference gas for CH_4-derived CO_2 and the N_2O measurement, respectively (Fig. 3). This enables simultaneous improvement and monitoring of the reproducibility before the sample peak enters the IRMS. The standard deviation of the three flat-topped reference gas peaks preceding the sample is 0.029 ‰ for

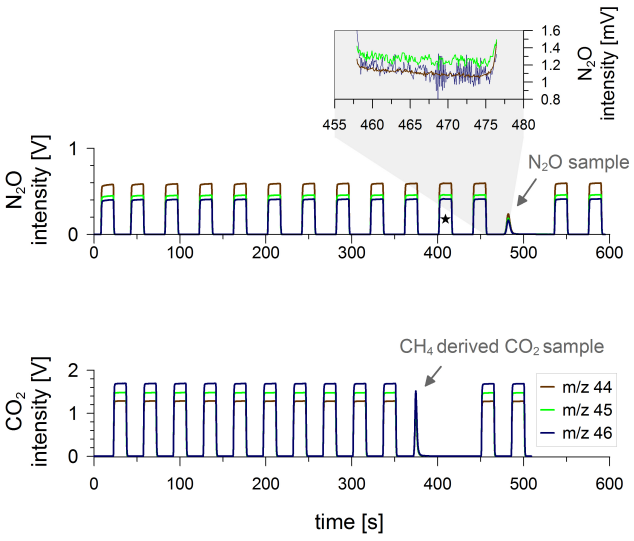

Fig. 3. Chromatograms with the three *m/z* 44, 45 and 46 traces for CH_4 (bottom panel) and of N_2O (top panel) measurements. The enlargement in the top panel shows the background before the N_2O sample peak in detail (units in mV). The flat-topped peaks in the main chromatograms are "on/off" peaks from pure N_2O and CO_2 reference gases. The chromatograms show the measurement of an ice core sample with low N_2O and CH_4 mixing ratios, typical for glacial periods. Reference gas peak 11 of the N_2O measurement (marked with star) includes a very small CO_2 remainder (not visible) stemming from system blank and incomplete CO_2 removal by the Ascarite. We use its isotopic composition to monitor the performance of the Ascarite trap (Fig. 1).

δ^{13}C-CO_2, 0.061 ‰ for δ^{15}N-N_2O and 0.086 ‰ for δ^{18}O-N_2O, respectively (average of 66 measurement sequences). These values refer to reference gas peak 8, 9 and 10 in the CH_4-derived CO_2 sequence and 9, 10 and 12 in the N_2O sequence (peak number 11 in the N_2O sequence is not considered due to the small contribution of CO_2 (caption of Fig. 3). The traces show baseline separation for ≥ 5 s between reference gas and sample peaks in all chromatograms, which is the time interval used for baseline determination as part of the peak integration parameters. Measurements of atmospheric and synthetic air mixtures with precisely referenced δ^{13}C-CH_4 (Sperlich et al., 2012) suggest this conditioning method of the IRMS showed no significant η effect (Brand, 2004) over δ^{13}C-CH_4 range of 5 ‰, reflecting the magnitude of δ^{13}C-CH_4 variability in firn and ice core samples (e.g. Fischer et al., 2008).

3.3 Excluding krypton interference

Krypton – which is abundant in the atmosphere at ~ 1 ppm (Aoki and Makide, 2005) – was found to co-elute from the GC column with CH_4 and interfere with the analysis of CH_4-derived CO_2 (Schmitt et al., 2013). The system described here deploys a post-combustion cryo-trap followed by a second GC column (Fig. 2). This combination ensures cryogenic

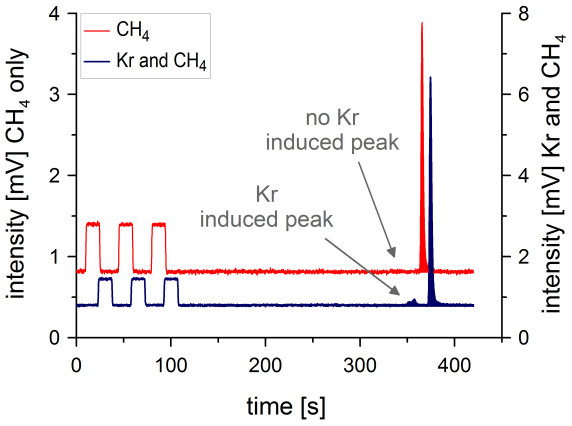

Fig. 4. A small krypton signal is visible when comparing the *m/z* 43 traces of δ^{13}C-CH_4 measurements in an atmospheric air mixture (dark-blue line, right axis) and in a pure CH_4 gas (red line, left axis), where the latter contains no Kr. Both peaks of CH_4 occur on *m/z* 43, while the baseline separated peak induced by remnant Kr occurs only in the atmospheric sample. To avoid an overlap of the displayed peaks, the chromatogram of the pure CH_4 is shifted by 15 s.

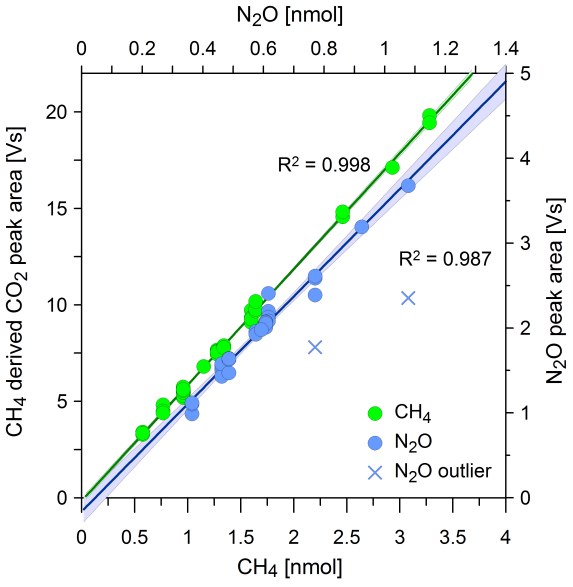

Fig. 5. Sample recovery. Green circles show the injected CH_4 amount [nmol] and the resulting IRMS peak area [Vs] as detected during bubble-free ice measurements with the injection of four different air mixtures in variable amounts. Blue circles display analogue information for N_2O. The two blue crosses show outliers of N_2O that suffered from a loss of IRMS peak area for unknown reasons. Both outliers are therefore not included in the calculation of the regression, which are shown with 95 % confidence interval.

separation of CH_4-derived CO_2 and Kr in T5 as only fractions of the Kr get trapped in T5 at LN_2 temperature. After the cryogenic separation, GC 2 ensures chromatographic separation of CH_4-derived CO_2 and remaining Kr. To test the Kr impact, the CO_2 gas configuration was modified to monitor the mass triplet *m/z* 43/44/45 during a CH_4 measurement instead of *m/z* 44/45/46 (Fig. 4). This test showed a crippled peak from $^{86}Kr^{++}$ on *m/z* 43 which precedes the δ^{13}C-CH_4 measurement of atmospheric air with baseline separation of 10 s between Kr- and the CH_4-derived CO_2 peak on *m/z* 43 (Fig. 4). In this case, the sample peak produced a small signal on *m/z* 43, as can also be seen for the three reference gas peaks (pure CO_2) at the beginning of both sequences. In comparison, injections of pure CH_4 via V3 into T4 underwent exactly the same analytical steps in the GC-C-GC-IRMS section but did not show the crippled $^{86}Kr^{++}$ peak on *m/z* 43 at all (Fig. 4). This test identifies the crippled peak from $^{86}Kr^{++}$ in the air sample and proves that our δ^{13}C-CH_4 measurements are not affected by Kr interferences.

3.4 Shot noise

We apply the approach of Merritt et al. (1994) to calculate the shot noise for the different analytes and the average peak areas of reference gases and samples. We calculated a shot-noise range on the 1-σ level of 0.04–0.05 ‰ for δ^{13}C-CH_4, 0.11–0.17 ‰ for δ^{15}N-N_2O and 0.15–0.22 ‰ for δ^{18}O-N_2O. The calculated shot-noise ratio may therefore explain between 40 and 50 % of the measurement uncertainty for δ^{13}C-CH_4 and between 20 and 29 % and 21–31 % of the uncertainty of the δ^{15}N and δ^{18}O measurements of N_2O, respectively. The remaining uncertainty is most likely based on the variability of the sample preparation. Generally, the shot-noise ratio is larger for N_2O than for CO_2 due to the lower abundances of the rare isotope (1.1 % ^{13}C, 0.37 % ^{15}N and 0.201 % ^{18}O, e.g. Sessions, 2006) and the signal intensity of N_2O as compared to CH_4-induced CO_2, due to lower mixing ratios (e.g. Schilt et al., 2010) and ionization efficiency (Friedli and Siegenthaler, 1988; Ghosh and Brand, 2004).

3.5 Sample recovery of injected air standards

Figure 5 shows the sample recovery as the response of the system to sample size variations between 0.5 and 3.2 nmol CH_4 and 0.3 and 1.1 nmol N_2O. The measurements are based on the extractions of air samples between 20 and 70 mL, respectively (Sect. 3.7). Since the valves to route the MFC injection of reference gases into the extraction line were manually controlled, a small variability of the applied volume and hence in IRMS peak area of CH_4-induced CO_2 and N_2O could not be avoided. The linear regression of the average IRMS peak area over the injected sample size shows an R^2 of 0.998 and 0.987 for CH_4 and N_2O, respectively. We therefore conclude the extraction unit and the components of the GC-C-GC-IRMS system responded linearly to sample size variability, indicating appropriate system design and timing steps enabling quantitative analysis within the expected sample size range.

3.6 System blank tests

The detected system blanks represent an integrated signal of system leakage and contamination within the analytical gas streams, but more importantly, they represent ice-sample-specific leakage through the melt vessel gasket as well as sample remnants from incomplete extractions. Another theoretical source of N_2O blank peaks is the microbial production of N_2O from NO_3 and NH_4. This N_2O production might take place after the ice core extraction, while the melted sample remains in the melt vessel (Jochen Schmitt, personal communication, 2013). However, we have no evidence for this process and cannot distinguish between all contributing sources.

We compared the IRMS peak areas of each blank test to the IRMS peak areas of the preceding ice core sample for 35 ice core measurements, and found blank peak areas with an average size of 1.5 and 3.0 % of the preceding CH_4 and N_2O sample, respectively. The N_2O blank size neither correlates with the CH_4 blank nor could any anomalous signal be detected on the TCD, precluding leakage from laboratory air. We speculate that the higher N_2O blank values resulted from ice core air remnants due to higher solubility as compared to CH_4 or in situ production during melting. In fact, 12 out of 35 blank tests showed a peak area that exceeded 5 % of the peak area of the preceding N_2O sample. The blank tests of the other 23 ice core samples averaged to 1.1 % of the sample peak area. These tests might indicate limitations in the extraction efficiency for N_2O during the melt extraction as compared to the extraction efficiency of CH_4. Because the isotope ratios of such small peaks are not unambiguously detectable, we do not apply blank corrections to our isotope measurements.

During the test phase of the setup, we installed a helium flow of 200 mL min^{-1} to strip dissolved gases from the melted ice core sample after the majority of the gases have been extracted as described in Sect. 2.6.1. Unlike Behrens et al. (2008) and Bock et al. (2010a), we pumped on the extraction line at the downstream end of T2 to absorb the sample gases on T2 while removing the helium for 5–10 min. Measurements of ice core samples that were extracted with the stripping method did not show a significant blank reduction or a reduced variability of isotopic analysis for CH_4 and N_2O, and did not conclude a more efficient extraction method. The stripping technique was thus excluded from the setup.

3.7 System calibration with bubble-free ice measurements

We follow the approach of Sowers and Jubenville (2000), Bock et al. (2010a) and Sapart et al. (2011) to calibrate our ice core extraction systems using artificial, bubble-free ice (BFI). We measured a total number of 35 air standard extractions over eight BFI samples. The first air standard was injected over the frozen BFI sample in the evacuated melt vessel. The BFI was then melted completely before the extraction was started. After the first extraction, the melted BFI sample was kept in the melt vessel under vacuum. Air standards were then injected over the melted BFI sample and the extraction started after 2 min. The air standards were taken from four different air mixtures (GIS, AL, NEEM, NOAA, Table 1), each with different isotopic composition and different mixing ratios of CH_4 and N_2O, respectively. By analysing between 20 and 70 mL (STP) of the air standards, the calibration experiments covered a large range of sample sizes including the amount of sample air to be expected from the extraction of 200 to 500 g of glacial and interglacial ice core samples (Fig. 6).

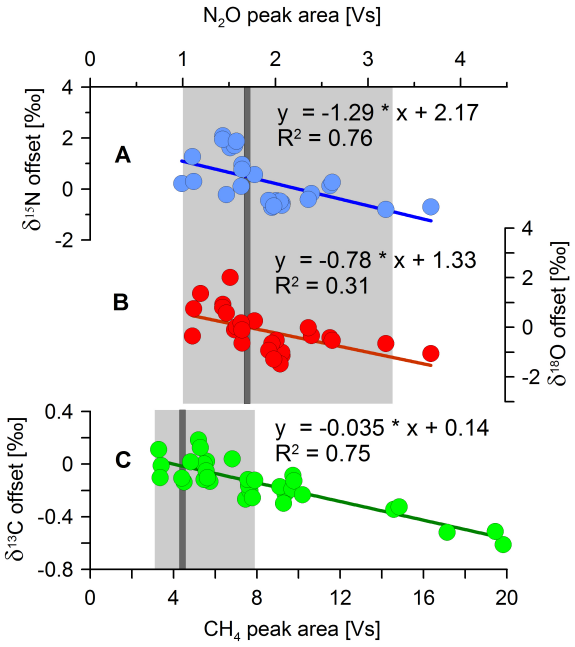

Fig. 6. Impact of sample size variability on the isotopic composition of δ^{15}N-N_2O **(A)**, δ^{18}O-N_2O **(B)** and δ^{13}C-CH_4 **(C)**. The offsets in isotopic composition of CH_4 and N_2O were determined in 33 and 26 BFI extractions, respectively. The dark-grey lines indicate the IRMS peak area of the reference gas measurements (GIS), which were used to reference the BFI samples to the respective isotope scales. The shaded zones indicate the IRMS peak area range of ice core sample measurements. Coloured lines display the linear regressions that are used to correct the isotopic composition of sample measurements for the difference in IRMS peak area between sample and reference gas.

Two BFI samples that were produced in the same BFI batch contained dissolved gases that only affected their first BFI measurement that included their melt process. This observation is in line with the description of Bock et al. (2010a), who found dissolved gases in BFI samples even though the BFI contained no visible gas inclusions. The stability of the consecutive extractions over melted BFI showed that a melted sample was completely degassed by the previous air extraction. Changing the air standards of two

consecutive injections showed no memory effect in the isotope ratios of CH_4 or N_2O, highlighting quantitative extraction. A significantly increased variability in both N_2O isotope ratios occurred during two days of BFI measurements. The data of these measurements were excluded, resulting in less N_2O data of BFI measurements as compared to CH_4 (Fig. 6). We speculate that this effect is based on disequilibration effects inside the Hayesep D in trap T2 after longer standby times. Regular use of T2 or pre-conditioning it with adsorption–desorption cycles in case T2 has not been used for a while stabilized the N_2O isotope ratios. However, CH_4 measurements were unaffected. The system returned to stable analysis the following day.

The isotope ratio of the BFI measurements was referenced via reference gas injections of 40 mL (GIS) to the respective international isotope scales. The linear regression of the isotope ratio offset versus the sample peak size is used to correct for differences in analyte amount of ice-core-air extractions from the melt vessel and reference gas extractions from T1 (Fig. 6). We find no significant isotope fractionation between the extractions from T1 and from the melt vessel for experiments with identical amounts of analytes. We therefore conclude that there is no significant offset between the extraction of reference gases from T1 and ice core samples from the melt vessel, and that the occurring fractionation is only based on the analyte amount. The correction according to the linear regression (Fig. 6) therefore covers the necessary corrections that relate all samples to the isotope scales as defined by 40 mL of the reference gas (Sect. 2.3). The sample-size-corrected BFI measurements show a standard deviation (1σ) of 0.09 ‰ for δ^{13}C-CH_4, 0.5 ‰ for δ^{15}N-N_2O and 0.7 ‰ for δ^{18}O-N_2O.

3.8 Quality control standard measurements

One QCS measurement was included in each routine for ice core measurements (Table 2). The QCS were varied in size and evaluated as an unknown sample with corrections for size- and system variability (Sect. 3.7). The results of 17 QCS measurements for δ^{13}C-CH_4, δ^{15}N-N_2O and δ^{18}O-N_2O of the QCS from an ice core measurement campaign are plotted in the performance chart (Fig. 7). Because the BFI tests showed no detectable isotope fractionation between the BFI extractions from the melt vessel and the reference gas extractions from T1, we consider the QCS measurements representative to indicate the magnitude of the measurement uncertainty that is inherent to the analysis of ice core samples. The standard deviation of the QCS measurements is therefore an important measure for the precision of the system. The estimated measurement uncertainty for δ^{13}C-CH_4 is 0.08 ‰ and 0.6 ‰ for both δ^{15}N-N_2O and δ^{18}O-N_2O, based on the 1σ standard deviation of the QCS measurements.

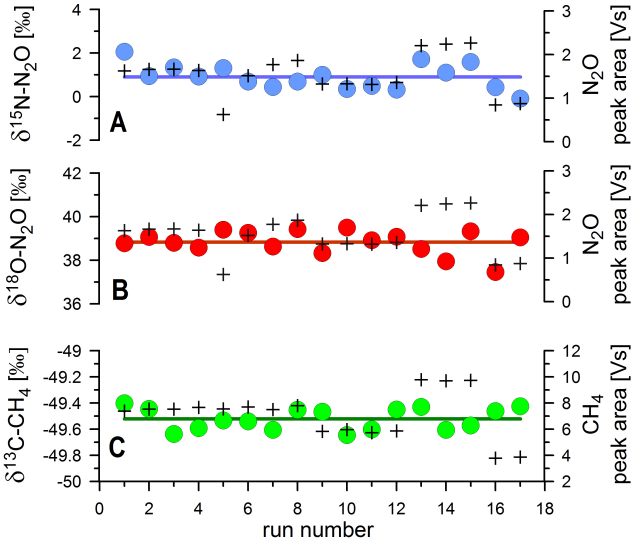

Fig. 7. Results of QCS measurements. The circles of the performance chart display the isotope ratio measurements of δ^{15}N-N_2O **(A)**, δ^{18}O-N_2O **(B)** and δ^{13}C-CH_4 **(C)** as determined during the QCS measurements by injecting variable amounts of AL. The crosses relate to the y axis on the right-hand side and indicate the IRMS peak area of the respective measurement. The lines show the average δ values of the measurements.

3.9 Reproducibility of ice core measurements

We measured 13 ice core samples (200–500 g) from the EUROCORE and NEEM ice core (gas age 657–1766 AD) to compare the performance of the setup with published δ^{13}C-CH_4 data (Fig. 8). Eleven of these samples are measured as replicates that are divided into four groups of 2–4 samples with a maximum age difference within each group of less than 14 yr. These sample groups can be assumed to contain air of similar composition (Buizert et al., 2012). The pooled standard deviation for δ^{13}C-CH_4 in these 11 samples of 0.07 ‰ is a representative measure for the reproducibility of ice core measurements. Unfortunately, we cannot provide the corresponding N_2O data of these samples as the measurement routine for N_2O measurements was not fully developed at the time these ice core measurements were done.

3.10 Precision of the setup

Multiple gases which differ in the isotopic composition as well as in the mixing ratio of CH_4 and N_2O were injected over BFI to calibrate the system. One measurement of AL in variable amounts was included as QCS measurement during every day of ice core measurements to monitor the performance of the analytical setup including the data processing. Finally, we showed the reproducibility for the δ^{13}C-CH_4 measurements of the setup by the pooled standard deviation of 11 pre-industrial ice core samples between 200 and 500 g. We find the uncertainty estimate based on the analysis of ice

core samples most representative. However, its comparability is restricted because each ice core sample represents a unique air mixture that may be affected by atmospheric variability and the stochastic nature of bubble trapping. Therefore, even two adjacent ice core samples are not necessarily 100 % identical. This problem of system calibration can be circumvented by repeated analysis of reference gases from pressurized tanks. For the δ^{13}C-CH_4 measurement, the uncertainty estimates as derived from the BFI measurements, the QCS measurements and the pooled standard deviation of ice core sample measurements are in good agreement, suggesting that a realistic measurement uncertainty is estimated by all three methods. For the isotopic analysis of N_2O, the uncertainty estimate of the BFI and the QCS measurements also agree well. Based on the good match of the uncertainty estimates discussed for δ^{13}C-CH_4, we suggest that the uncertainty of N_2O measurements can reliably be estimated from the BFI and QCS measurements. For all measured parameters, we chose to state the uncertainty with the highest value, independent of the method from which it was derived. We therefore conclude a measurement uncertainty of 0.09 ‰ for δ^{13}C-CH_4 (BFI), 0.6 ‰ for δ^{15}N-N_2O (QCS) and 0.7 ‰ for δ^{18}O-N_2O (BFI), which is comparable to or better than those of Sowers et al. (2003), Ferretti et al. (2005), Schaefer and Whiticar (2007), Behrens et al. (2008), Sowers (2009), Sapart et al. (2011) and Melton et al. (2011b).

3.11 Comparison to published ice core data and established systems

3.11.1 δ^{13}C-CH_4

We measured a total of 13 EUROCORE and NEEM ice core samples for δ^{13}C-CH_4 and compared our results with NEEM ice core data that were recently published by Sapart et al.(2012) as shown in Fig. 8. The data from Sapart et al. (2012) were corrected for the Kr effect, which was not known at the time of publication. The Kr-corrected IMAU data are between 0.15 and 0.88 ‰ more depleted in δ^{13}C-CH_4, depending on the CH_4 mixing ratio, where the highest correction was applied to the samples from the industrial period. Our data and the Kr-corrected data from Sapart et al. (2012) will be referred to as CIC and $IMAU_{Kr}$, respectively. We selected six data points of the $IMAU_{Kr}$ dataset between 677 and 1757 AD and measured between one and four samples per $IMAU_{Kr}$ data point on our setup. The mean gas age of the CIC and the respective $IMAU_{Kr}$ samples differed between 1 and 24 yr. Greenland ice core samples have been shown to integrate the atmospheric variability over a period of about 35 yr (Buizert et al., 2012). We therefore consider the compared samples to represent similar air samples.

CIC and $IMAU_{Kr}$ data show excellent agreement during five time intervals that cover a δ^{13}C-CH_4 range of nearly 2 ‰ (Fig. 8). However, we found a disagreement between $IMAU_{Kr}$ and the mean of four CIC samples (three Eurocore, one NEEM) during the δ^{13}C-CH_4 excursion reported by Sapart et al. (2012) at 964 AD, where the $IMAU_{Kr}$ sample is more enriched in δ^{13}C-CH_4 by ∼ 1 ‰. Between 900 and 1000 AD, three $IMAU_{Kr}$ samples agree well, which rules out that the disagreement is based on one outlier. Since we can exclude Kr interference as the reason for the offset, we speculate that the differences between CIC and $IMAU_{Kr}$ are due to differences in the ice core samples, the sample preparation or the ice extraction technique.

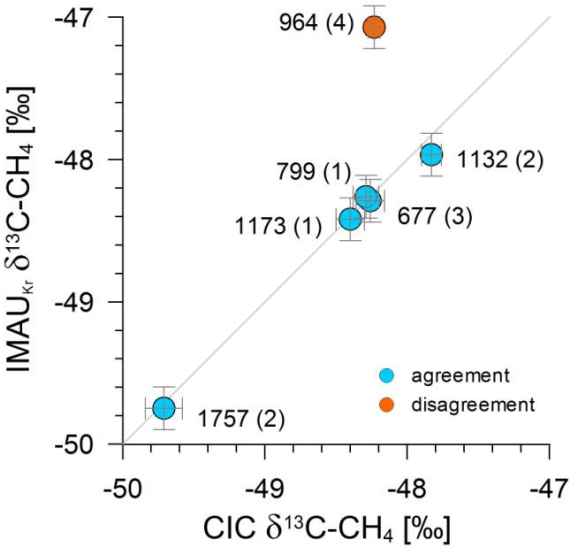

Fig. 8. Comparison of CIC and $IMAU_{Kr}$ δ^{13}C-CH_4 ice core data (the index in $IMAU_{Kr}$ indicates the data have been corrected for the Kr effect). Blue circles indicate data comparison of time sections where good agreement was found. The orange circle indicates the comparison where CIC and $IMAU_{Kr}$ found a disagreement of ∼ 1 ‰. Error bars indicate the measurement uncertainty or the average of the measurements used for the laboratory comparison. Bracketed numbers indicate the numbers of samples measured at CIC for the respective comparison, while numbers without brackets display the time (AD) of the $IMAU_{Kr}$ samples.

At about 950 and 1000 AD, Rhodes et al. (2013) show several spikes of excess CH_4, measured on a shallow NEEM ice core. The strongest of these CH_4 artefacts (+78 ppb) was detected in a depth of 272.1 m, which is close to the samples of Sapart et al. (2012) from 964 and 1009 AD (269.5 m and 278.3 m, respectively) but even closer to the depth of the one NEEM sample that was measured at CIC for this intercomparison (272.8 m). Note that the samples of Rhodes et al. (2013) were taken from a shallow core at NEEM, while the discussed NEEM samples are taken from the main core. The age–depth relation may vary slightly between the two cores, which hampers drawing unambiguous conclusions.

One hypothesis is that impurities in the ice are related to excess CH_4 (Rhodes et al., 2013) and thus possibly caused the disagreement between CIC and $IMAU_{Kr}$. While ice core layers that contained visible particles were removed during

sample preparation at CIC, small particles were observed and retained within one $IMAU_{Kr}$ sample that shows the disagreement. However, adjacent $IMAU_{Kr}$ samples with and without visible particles agree well in δ^{13}C-CH_4, as is confirmed from other depth ranges, thereby questioning the hypothesis that particles in the ice necessarily create artefacts in δ^{13}C-CH_4. Thus, the link between particles and δ^{13}C-CH_4 offset remains speculative.

One analytical difference between CIC and $IMAU_{Kr}$ is the technique to extract air from ice core samples. While a continuous melt-extraction technique is used at CIC, $IMAU_{Kr}$ data are based on a dry-extraction technique (Sapart et al., 2011). Both techniques are optimized for high extraction efficiency, and both techniques are shown to produce very similar results. It is therefore unlikely that conceptual differences of the extraction techniques alone caused the observed disagreement in δ^{13}C-CH_4.

Because the data comparison between CIC and $IMAU_{Kr}$ shows excellent agreement during all other time intervals, we find our setup suitable for δ^{13}C-CH_4 measurements in ice core samples. A δ^{13}C-CH_4 record of firn air samples was measured on our setup and also shows very good agreement with the results from other systems as published by Sapart et al. (2013).

3.11.2 δ^{15}N-N_2O and δ^{18}O-N_2O

A flask intercomparison study for N_2O isotope ratios in three different gas mixtures was conducted to compare our setup to the setup described by Sapart et al. (2011). The air mixtures used for this test varied by ~ 7 and ~ 6 ‰ in δ^{15}N and δ^{18}O, respectively (Table 1). The results for all gases showed excellent agreement within the uncertainty of the measurements and were published earlier (Sapart et al., 2011).

So far, intercomparison measurements on isotope ratios of N_2O ice core samples have not been made in the ice core community, and data for the time period of our δ^{13}C-CH_4 comparison measurements (657–1766 AD) are lacking. We therefore cannot give an ice core intercomparison at this stage but emphasize the need for such a study in the future.

4 Summary and conclusions

We introduced Aurolite as reliable catalyst for the oxidation of CO. Based on our test we conclude that Aurolite is useful to produce CO-free air for reference gas mixing purposes. We expect that Aurolite could also be used to analyse δ^{14}C-CO; however, more tests would be required to prove this hypothesis. We described our setup to measure δ^{13}C-CH_4, δ^{15}N-N_2O and δ^{18}O-N_2O isotope ratios in air- and ice core samples and thoroughly discussed its performance and measurement uncertainty based on bubble-free ice and quality control standard measurements. We proved the reproducibility of the analytical system and the suggested data-processing method based on detailed experiments with sample amounts that can be expected in 200–500 g of glacial and interglacial ice core samples. We furthermore compared our ice core measurement for δ^{13}C-CH_4 with published data which prove that our setup is capable of highlighting small yet significant isotope variations with excellent precision. A previously published intercomparison of isotope measurements of N_2O in reference gases proved the described setup to be in very good agreement with established systems. A high-resolution dataset of δ^{15}N-N_2O and δ^{18}O-N_2O measurements from ice core samples between 657 and 1766 AD is not available for intercomparison. However, we discussed measurement control strategies analogue to our δ^{13}C-CH_4 measurements that suggest our setup is suitable to reliably measure the isotopic composition of N_2O in ice core samples. We conclude that the precision of our setup for δ^{13}C-CH_4, δ^{15}N-N_2O and δ^{18}O-N_2O measurements is 0.09, 0.6 and 0.7 ‰, respectively. Especially the excellent precision of our setup for δ^{13}C-CH_4 and its independence of Kr interference make our setup suitable to analyse the variability of the interhemispheric gradient of CH_4 and of small changes of δ^{13}C-CH_4 in high temporal resolution. The described setup enables measurement of two samples per day, which allows production of large datasets in future. Upcoming work should also include the harmonization of similar analytical systems and sample preparation protocols to minimize interlaboratory offsets as well as the investigation of measurement artefacts.

Acknowledgements. We would like to thank the field teams that took the EUROCORE and NEEM samples. NEEM is directed and organized by the Centre for Ice and Climate at the Niels Bohr Institute and the US NSF, Office of Polar Programs. It is supported by funding agencies and institutions in Belgium (FNRS-CFB and FWO), Canada (NRCan/GSC), China (CAS), Denmark (FIST), France (IPEV, CNRS/INSU, CEA and ANR), Germany (AWI), Iceland (RannIs), Japan (NIPR), Korea (KOPRI), the Netherlands (NWO/ALW), Sweden (VR), Switzerland (SNF), the United Kingdom (NERC) and the United States (US NSF, Office of Polar Programs). We greatly appreciated helpful discussions with Hinrich Schaefer, Katja Riedel, Peter Franz and Gordon Brailsford from NIWA and with Willi Brand from the MPI-BGC. We are grateful for the support of Colleen Templeton, and would like to acknowledge the two referees Jochen Schmitt and Jochen Rudolph for their valuable contributions, which considerably improved the manuscript.

Edited by: R. Koppmann

References

Anicich, V. G.: Evaluated bimolecular ion-molecule gas-phase kinetics of positive-ions for use in modeling planetary-atmospheres, cometary comae, and interstellar clouds, J. Phys. Chem. Ref. Data, 22, 1469–1569, 1993.

Aoki, N. and Makide, Y.: The concentration of krypton in the atmosphere – its revision after half a century, Chem. Lett., 34, 1396–1397, doi:10.1246/cl.2005.1396, 2005.

Behrens, M., Schmitt, J., Richter, K. U., Bock, M., Richter, U. C., Levin, I., and Fischer, H.: A gas chromatography/combustion/isotope ratio mass spectrometry system for high-precision $\delta^{13}C$ measurements of atmospheric methane extracted from ice core samples, Rapid Commun. Mass Sp., 22, 3261–3269, doi:10.1002/rcm.3720, 2008.

Bock, M., Schmitt, J., Behrens, M., Möller, L., Schneider, R., Sapart, C., and Fischer, H.: A gas chromatography/pyrolysis/isotope ratio mass spectrometry system for high-precision δD measurements of atmospheric methane extracted from ice cores, Rapid Commun. Mass Sp., 24, 621–633, doi:10.1002/rcm.4429, 2010a.

Bock, M., Schmitt, J., Möller, L., Spahni, R., Blunier, T., and Fischer, H.: Hydrogen isotopes preclude marine hydrate CH_4 emissions at the onset of Dansgaard-Oeschger events, Science, 328, 1686–1689, doi:10.1126/science.1187651, 2010b.

Brand, W. A.: Precon: A fully automated interface for the pre-GC concentration of trace gases in air for isotopic analysis, Isot. Environ. Healt. S., 31, 277–284, doi:10.1080/10256019508036271, 1995.

Brand, W. A.: Mass spectrometer hardware for analyzing stable isotope ratios, in: Handbook of stable isotope analytical techniques, Vol. 1, edited by: Groot, P. A., Elsevier B. V., Amsterdam, 835–856, 2004.

Brenninkmeijer, C. A. M.: Measurement of the abundance of ^{14}CO in the atmosphere and the $^{13}C/^{12}C$ and $^{18}O/^{16}O$ ratio of atmospheric CO with applications in New-Zealand and Antarctica, J. Geophys. Res.-Atmos., 98, 10595–10614, doi:10.1029/93jd00587, 1993.

Brenninkmeijer, C. A. M., Janssen, C., Kaiser, J., Rockmann, T., Rhee, T. S., and Assonov, S. S.: Isotope effects in the chemistry of atmospheric trace compounds, Chem. Rev., 103, 5125–5161, doi:10.1021/cr020644k, 2003.

Buizert, C., Martinerie, P., Petrenko, V. V., Severinghaus, J. P., Trudinger, C. M., Witrant, E., Rosen, J. L., Orsi, A. J., Rubino, M., Etheridge, D. M., Steele, L. P., Hogan, C., Laube, J. C., Sturges, W. T., Levchenko, V. A., Smith, A. M., Levin, I., Conway, T. J., Dlugokencky, E. J., Lang, P. M., Kawamura, K., Jenk, T. M., White, J. W. C., Sowers, T., Schwander, J., and Blunier, T.: Gas transport in firn: Multiple-tracer characterisation and model intercomparison for NEEM, Northern Greenland, Atmos. Chem. Phys., 12, 4259–4277, doi:10.5194/acp-12-4259-2012, 2012.

Carter, J. F. and Barwick, V. J.: Good practice guide for isotope ratio mass spectrometry, 1st Edn., 1–48, ISBN 978-0-948926-31-0, 2011.

Coplen, T. B., Brand, W. A., Gehre, M., Groning, M., Meijer, H. A. J., Toman, B., and Verkouteren, R. M.: After two decades a second anchor for the VPDB $\delta^{13}C$ scale, Rapid Commun. Mass Sp., 20, 3165–3166, doi:10.1002/rcm.2727, 2006.

Cullis, C. F. and Willatt, B. M.: Oxidation of methane over supported precious metal-catalysts, J. Catal., 83, 267–285, doi:10.1016/0021-9517(83)90054-4, 1983.

Date, M., Ichihashi, Y., Yamashita, T., Chiorino, A., Boccuzzi, F., and Haruta, A.: Performance of Au/TiO_2 catalyst under ambient conditions, Catal. Today, 72, 89–94, doi:10.1016/s0920-5861(01)00481-3, 2002.

DesMarais, D. J.: Variable-temperature cryogenic trap for separation of gas-mixtures, Anal. Chem., 50, 1405–1406, doi:10.1021/ac50031a056, 1978.

Ferretti, D. F., Miller, J. B., White, J. W. C., Etheridge, D. M., Lassey, K. R., Lowe, D. C., Meure, C. M. M., Dreier, M. F., Trudinger, C. M., van Ommen, T. D., and Langenfelds, R. L.: Unexpected changes to the global methane budget over the past 2000 years, Science, 309, 1714–1717, doi:10.1126/science.1115193, 2005.

Fischer, H., Behrens, M., Bock, M., Richter, U., Schmitt, J., Loulergue, L., Chappellaz, J., Spahni, R., Blunier, T., Leuenberger, M., and Stocker, T. F.: Changing boreal methane sources and constant biomass burning during the last termination, Nature, 452, 864–867, doi:10.1038/nature06825, 2008.

Flückiger, J., Blunier, T., Stauffer, B., Chappellaz, J., Spahni, R., Kawamura, K., Schwander, J., Stocker, T. F., and Dahl-Jensen, D.: N_2O and CH_4 variations during the last glacial epoch: Insight into global processes, Global Biogeochem. Cy., 18, 14, Gb1020, doi:10.1029/2003gb002122, 2004.

Friedli, H. and Siegenthaler, U.: Influence of N_2O on isotope analyses in CO_2 and mass-spectrometric determination of N_2O in air samples, Tellus B, 40, 129–133, 1988.

Ghosh, P. and Brand, W. A.: The effect of N_2O on the isotopic composition of air-CO_2 samples, Rapid Commun. Mass Sp., 18, 1830–1838, doi:10.1002/rcm.1560, 2004.

Kato, S., Akimoto, H., Braunlich, M., Röckmann, T., and Brenninkmeijer, C. A. M.: Measurements of stable carbon and oxygen isotopic compositions of CO in automobile exhausts and ambient air from semi-urban Mainz, Germany, Geochem. J., 33, 73–77, 1999.

Loulergue, L., Schilt, A., Spahni, R., Masson-Delmotte, V., Blunier, T., Lemieux, B., Barnola, J. M., Raynaud, D., Stocker, T. F., and Chappellaz, J.: Orbital and millennial-scale features of atmospheric ch4 over the past 800,000 years, Nature, 453, 383–386, doi:10.1038/nature06950, 2008.

McPherson, J., Thompson, D., Pattrick, G., Holliday, R., Ramdayal, D., Khumalo, T., and Van der Lingen, E.: Commercial opportunities for gold catalysts, World Gold Conference 2009, Johannesburg, South Africa, 2009.

Melton, J. R., Schaefer, H., and Whiticar, M. J.: Enrichment in ^{13}C of atmospheric CH_4 during the younger dryas termination, Clim. Past., 8, 1177–1197, doi:10.5194/cp-8-1177-2012, 2011a.

Melton, J. R., Whiticar, M. J., and Eby, P.: Stable carbon isotope ratio analyses on trace methane from ice samples, Chem. Geol., 288, 88–96, doi:10.1016/j.chemgeo.2011.03.003, 2011b.

Merritt, D. A., Brand, W. A., and Hayes, J. M.: Isotope-ratio-monitoring gas-chromatography mass-spectrometry – methods for isotopic calibration, Org. Geochem., 21, 573–583, 1994.

Merritt, D. A., Freeman, K. H., Ricci, M. P., Studley, S. A., and Hayes, J. M.: Performance and optimization of a combustion interface for isotope ratio monitoring gas-chromatography mass-spectrometry, Anal. Chem., 67, 2461–2473, 1995.

Mitchell, L. E., Brook, E. J., Sowers, T., McConnell, J. R., and Taylor, K.: Multidecadal variability of atmospheric methane,

1000–1800 ce, J. Geophys. Res.-Biogeosci., 116, G02007, doi:10.1029/2010jg001441, 2011.

Rhodes, R. H., Faïn, X., Stowasser, C., Blunier, T., Chappellaz, J., McConnell, J., Romanini, D., Mitchell, L. E., and Brook, E. J.: Continuous methane measurements from a late holocene greenland ice core: Atmospheric and in-situ signals, Earth Planet. Sc. Lett., 368, 9–19, doi:10.1016/j.epsl.2013.02.034, 2013.

Röckmann, T. and Levin, I.: High-precision determination of the changing isotopic composition of atmospheric N_2O from 1990 to 2002, J. Geophys. Res.-Atmos., 110, D21304, doi:10.1029/2005jd006066, 2005.

Sapart, C. J., van der Veen, C., Vigano, I., Brass, M., van de Wal, R. S. W., Bock, M., Fischer, H., Sowers, T., Buizert, C., Sperlich, P., Blunier, T., Behrens, M., Schmitt, J., Seth, B., and Röckmann, T.: Simultaneous stable isotope analysis of methane and nitrous oxide on ice core samples, Atmos. Meas. Tech., 4, 2607–2618, doi:10.5194/amt-4-2607-2011, 2011.

Sapart, C. J., Monteil, G., Prokopiou, M., van de Wal, R. S. W., Kaplan, J. O., Sperlich, P., Krumhardt, K. M., van der Veen, C., Houweling, S., Krol, M. C., Blunier, T., Sowers, T., Martinerie, P., Witrant, E., Dahl-Jensen, D., and Röckmann, T.: Natural and anthropogenic variations in methane sources during the past two millennia, Nature, 490, 85–88, doi:10.1038/nature11461, 2012.

Sapart, C. J., Martinerie, P., Witrant, E., Chappellaz, J., van de Wal, R. S. W., Sperlich, P., van der Veen, C., Bernard, S., Sturges, W. T., Blunier, T., Schwander, J., Etheridge, D., and Röckmann, T.: Can the carbon isotopic composition of methane be reconstructed from multi-site firn air measurements?, Atmos. Chem. Phys., 13, 6993–7005, doi:10.5194/acp-13-6993-2013, 2013.

Schaefer, H. and Whiticar, M. J.: Measurement of stable carbon isotope ratios of methane in ice samples, Org. Geochem., 38, 216–226, doi:10.1016/j.orggeochem.2006.10.006, 2007.

Schaefer, H., Whiticar, M. J., Brook, E. J., Petrenko, V. V., Ferretti, D. F., and Severinghaus, J. P.: Ice record of $\delta^{13}C$ for atmospheric CH_4 across the younger dryas-preboreal transition, Science, 313, 1109–1112, doi:10.1126/science.1126562, 2006.

Schilt, A., Baumgartner, M., Schwander, J., Buiron, D., Capron, E., Chappellaz, J., Loulergue, L., Schupbach, S., Spahni, R., Fischer, H., and Stocker, T. F.: Atmospheric nitrous oxide during the last 140,000 years, Earth Planet. Sc. Lett., 300, 33–43, doi:10.1016/j.epsl.2010.09.027, 2010.

Schmitt, J., Seth, B., Bock, M., Fischer, H., Möller, L., Sapart, C. J., Prokopiou, M., Van der Veen, C., Röckmann, T., and Sowers, T.: On the interference of Kr during carbon isotope analysis of atmospheric methane using continuous flow combustion-isotope ratio mass spectrometry, Atmos. Meas. Tech., 6, 1425–1445, doi:10.5194/amt-6-1425-2013, 2013.

Sessions, A. L.: Isotope-ratio detection for gas chromatography, J. Sep. Sci., 29, 1946–1961, doi:10.1002/jssc.200600002, 2006.

Solomon, S., Qin, D., Manning, M., Alley, R. B., Berntsen, T., Bindoff, N. L., Chen, Z., Chidthaisong, A., Gregory, J. M., Hegerl, G. C., Heimann, M., Hewitson, B., Hoskins, B. J., Joos, F., Jouzel, J., Kattsov, V., Lohmann, U., Matsuno, T., Molina, M. J., Nicholls, N., Overpeck, J., Raga, G., Ramaswamy, V., Ren, J., Rusticucci, M., Somerville, R., Stocker, T. F., Whetton, P., Wood, R. A., and Wratt, D.: Climate change 2007: The physical science basis. Contribution of working group i to the fourth assessment report of the intergovernmental panel on climate change, 2007.

Sowers, T.: Late quaternary atmospheric CH_4 isotope record suggests marine clathrates are stable, Science, 311, 838–840, doi:10.1126/science.1121235, 2006.

Sowers, T.: Atmospheric methane isotope records covering the holocene period, Quaternary Sci. Rev., 29, 213–221, doi:10.1016/j.quascirev.2009.05.023, 2009.

Sowers, T. and Jubenville, J.: A modified extraction technique for liberating occluded gases from ice cores, J. Geophys. Res.-Atmos., 105, 29155–29164, 2000.

Sowers, T., Alley, R. B., and Jubenville, J.: Ice core records of atmospheric N_2O covering the last 106,000 years, Science, 301, 945–948, 2003.

Sowers, T., Bernard, S., Aballain, O., Chappellaz, J., Barnola, J. M., and Marik, T.: Records of the $\delta^{13}C$ of atmospheric CH_4 over the last 2 centuries as recorded in antarctic snow and ice, Global Biogeochem. Cy., 19, Gb2002, doi:10.1029/2004gb002408, 2005.

Sperlich, P., Guillevic, M., Buizert, C., Jenk, T. M., Sapart, C. J., Schaefer, H., Popp, T. J., and Blunier, T.: A combustion setup to precisely reference $\delta^{13}C$ and $\delta^{2}H$ isotope ratios of pure CH_4 to produce isotope reference gases of $\delta^{13}C$-CH_4 in synthetic air, Atmos. Meas. Tech., 5, 2227–2236, doi:10.5194/amt-5-2227-2012, 2012.

Sturm, P., Leuenberger, M., Sirignano, C., Neubert, R. E. M., Meijer, H. A. J., Langenfelds, R., Brand, W. A., and Tohjima, Y.: Permeation of atmospheric gases through polymer o-rings used in flasks for air sampling, J. Geophys. Res.-Atmos., 109, D04309, doi:10.1029/2003jd004073, 2004.

Umezawa, T., Aoki, S., Nakazawa, T., and Morimoto, S.: A high-precision measurement system for carbon and hydrogen isotopic ratios of atmospheric methane and its application to air samples collected in the western pacific region, J. Meteorol. Soc. Jpn., 87, 365–379, doi:10.2151/jmsj.87.365, 2009.

Verkouteren, R. M.: Preparation, characterization, and value assignment of carbon dioxide isotopic reference materials: Rms 8562, 8563, and 8564, Anal. Chem., 71, 4740–4746, doi:10.1021/ac990233c, 1999.

Walther, G., Cervera-Gontard, L., Quaade, U. J., and Horch, S.: Low temperature methane oxidation on differently supported 2 nm au nanoparticles, Gold Bull., 42, 13–19, doi:10.1007/BF03214901, 2009.

Werner, R. A. and Brand, W. A.: Referencing strategies and techniques in stable isotope ratio analysis, Rapid Commun. Mass Sp., 15, 501–519, 2001.